nature climate change

Article

https://doi.org/10.1038/s41558-023-01852-9

Thunderstorm straight line winds intensify with climate change

In the format provided by the authors and unedited

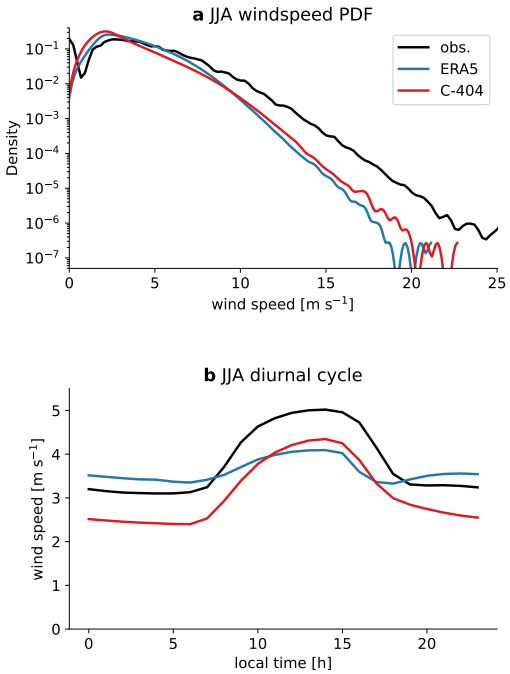

Fig. S 1: **C-404 improves the representation of strong wind and the diurnal cycle of wind in the central U.S. during JJA compared to ERA5.** Probability density function (a) and average diurnal cycle (b) of hourly wind speed in the central U.S. during JJA from observations (obs., black), ERA5 (blue), and C-404 (red) between 1980–2020.

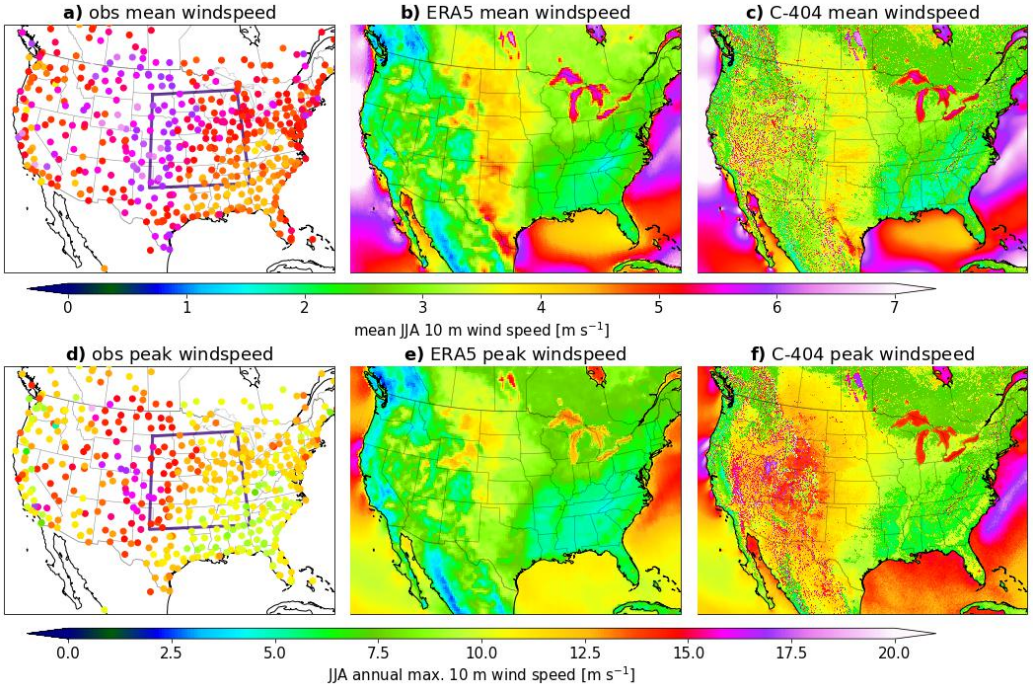

Fig. S 2: **JJA mean (a–c) and average annual maximum hourly (d–e) 10 m wind speed in station observations (first row), ERA5 (middle row), and C404 simulations (right row).**

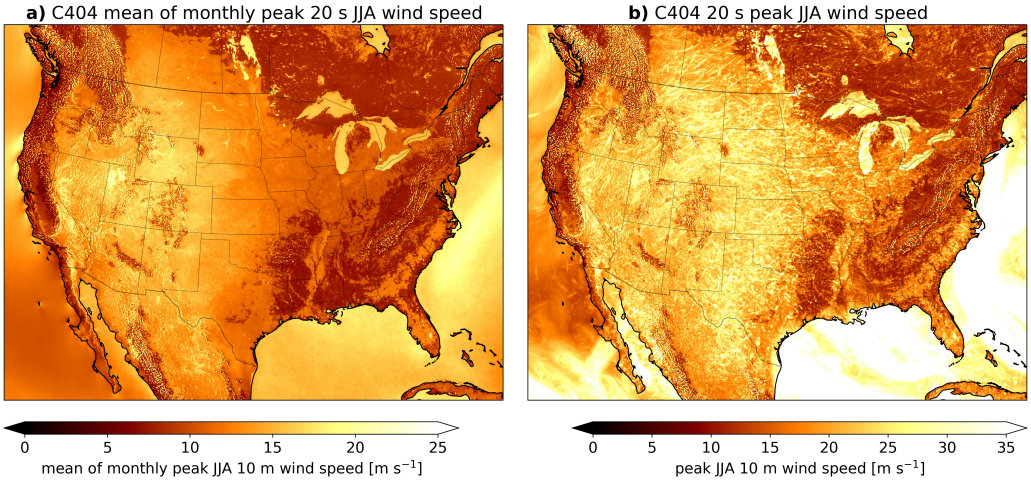

Fig. S 4: **Annual JJA maximum (a) and all time JJA maximum simulated 20 s wind speed.**

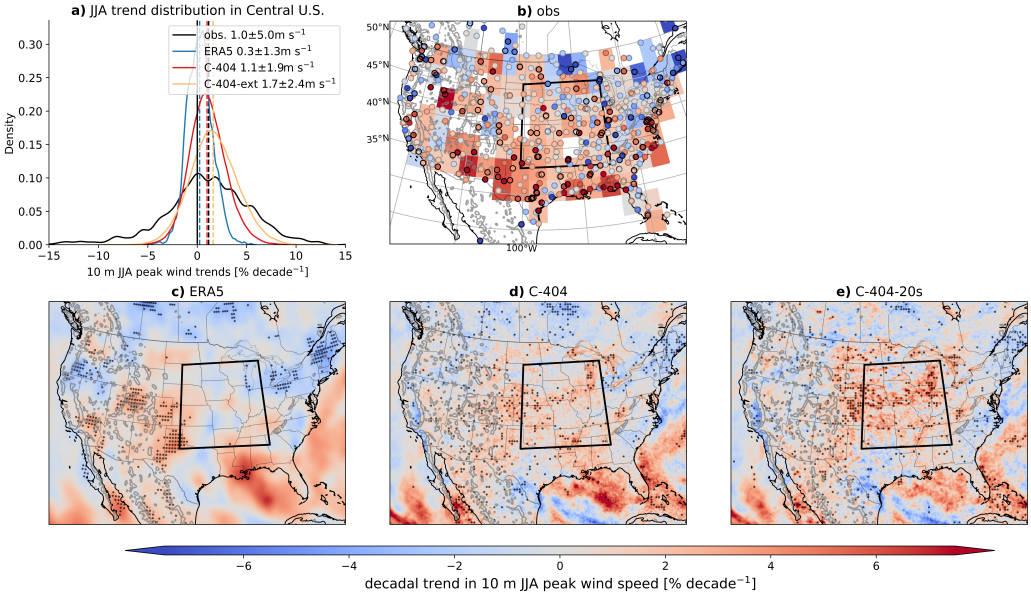

Fig. S 5: **JJA peak wind speed trends across the central U.S. and the Contiguous United States (CONUS).** Probability density function of linear trend estimates of maximum JJA wind speed at station locations in the central U.S. (A). JJA maximum wind speed trends from station observations (circles). Circles with black outlines show significant changes (two-sided p=0.05 Wald Test with t-distribution). Colored contours show average station trends in $3° \times 3°$ degree areas. Grid cell-based maximum JJA wind speed estimates from ERA5 (C), C-404 (D), and C-404-20s (E) datasets. Black dots are showing significant changes (two-sided p=0.05 Wald Test with t-distribution). The black polygon in the maps shows the location of the central U.S.

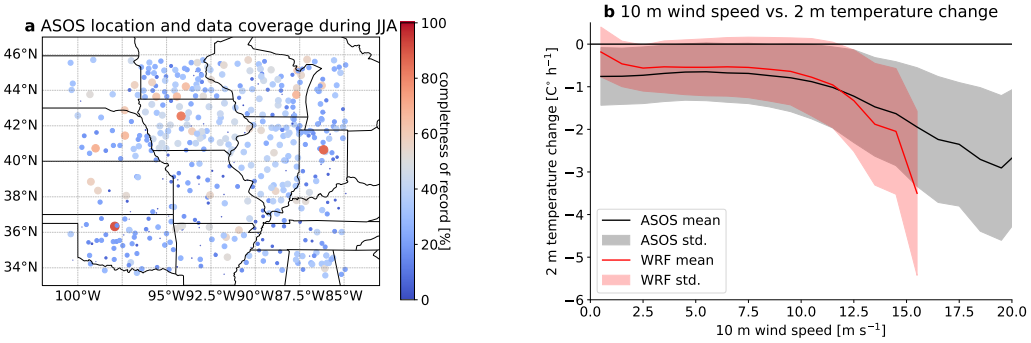

Fig. S 6: **Dependents of temperature change on wind speed intensity.** The right panel shows the observed (black; based on ASOS station data) and simulated (red) relationship between temperature change and wind speed during JJA in the central U.S. before or during high wind speeds events. The map on the left shows the location and completeness of station records from the ASOS network.

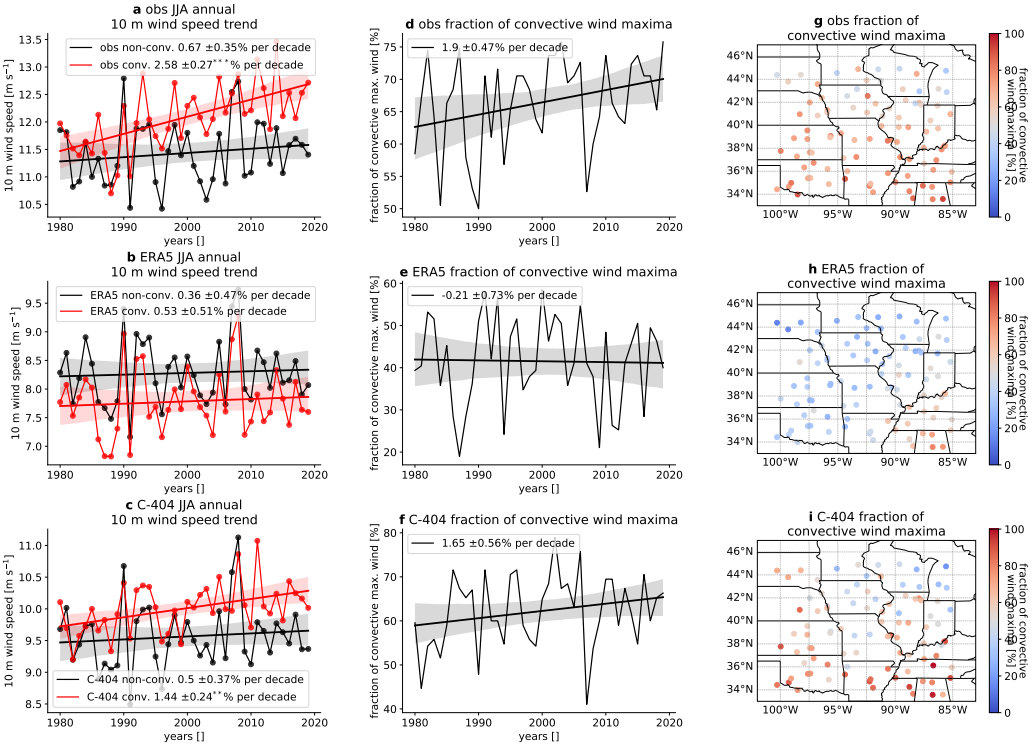

Fig. S 7: **The majority of JJA wind extremes in the Central U.S. are related to convection and their intensity increased over time.** Spatial averaged (over HadISD stations) JJA annual maximum wind speed considering maxima that occurred underneath or in the vicinity of a cold cloud shield (red lines and circles) or away from cold clouds (black lines and circles) for HadISD observations, ERA5, and C-404 data (a–c respectively). Lines in a–f show a least square error linear regression and contours show its two-sided 95 % confidence intervals. Fraction of stations where convective winds were the maximum observed wind in JJA (d–f). Lines and shadings in a–f show linear trend estimates and their uncertainty. The legend in a–c shows linear trends, their standard deviation, and statistical significance (*/**/** mean p-values of 0.05/0.01/0.005). The maps in g–i show the fraction of JJA maximum wind speeds related to convection.

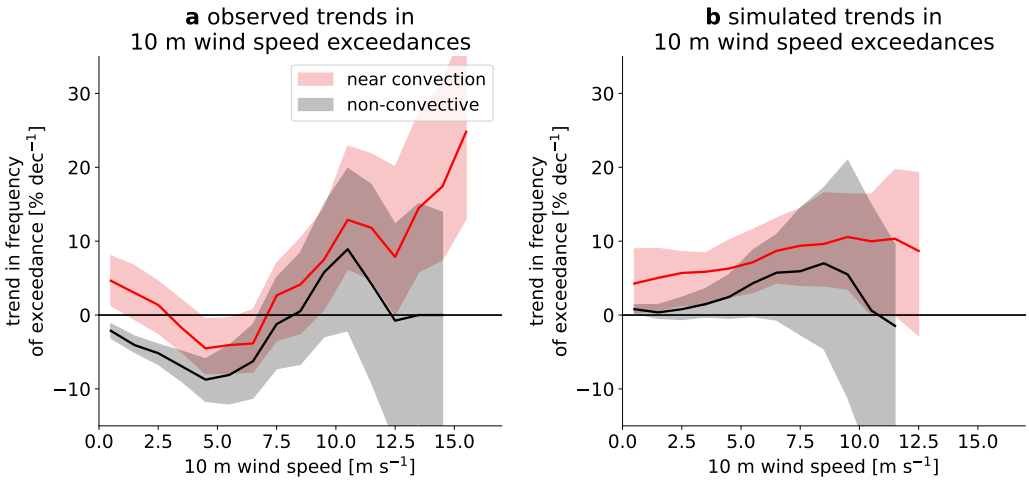

Fig. S 8: **Heavier wind speeds that occur near convection increased faster in frequency than weaker wind speeds.** Trend estimates in frequency exceedances as a function of wind speeds. The number of hours in each JJA season that exceed a certain wind speed (x-axis) across all stations in the Central U.S. are used to calculate relative frequency trend estimates. The trend estimates are based on Theil-Sen slopes for time series that have on average more than 10 hours per JJA (accumulated over all stations) that exceed the threshold. Thick lines show the best estimate while contours show the 95th confidence interval.

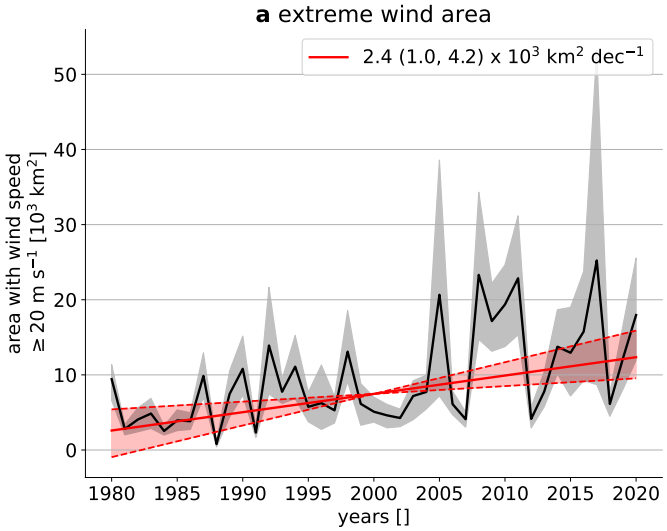

Fig. S 9: **The region affected by simulated SLW 4.8±1.2-folded during the last 40-years.** Accumulated JJA area affected by wind speeds larger than $20\,\mathrm{m\,s^{-1}}$. The gray shading shows the 10 to 90 percentile range of a 1,000-member bootstrap ensemble and the black line shows the median. All data in this figure corresponds to convective areas under cold cloud shields (see methods for more details). A Theil-Sen slope estimate (solid red line) and its 95th percentile confidence interval (red dashed lines) are shown additionally to the best slope estimate including its lower and upper bound.

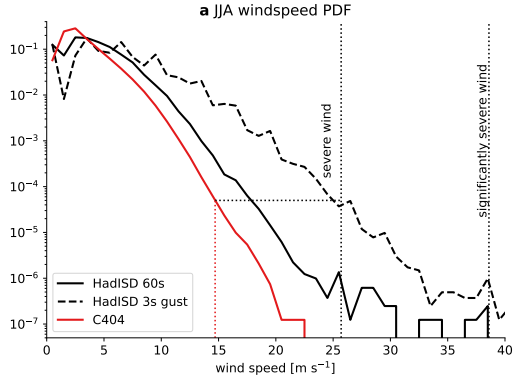

Fig. S 10: **I use gust probability thresholds to estimate the approximate wind speed of severe and significant severe winds speeds in the C404 simulations.** Three-second gusts are estimated by applying a gust factor of 1.49[?] to the HadISD mean wind speed between 1980–2020 (dashed line). The corresponding probability density function (PDF) is used to find the observed probabilities of severe and significant severe wind events (vertical black dashed lines). These probabilities are used to select the correspondent wind speed from the C404 PDFs. For instance, severe winds are defined as 3-s gusts faster than 25.7 m s^{-1}, which corresponds to 14.8 m s^{-1} in C404.

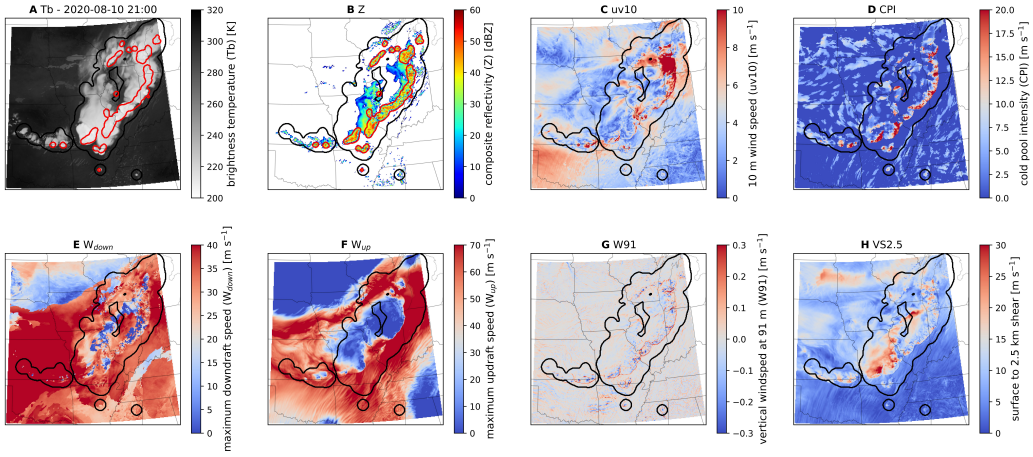

Fig. S 11: **Selection of potential areas with straight line winds on the example of a Derecho on August 10, 2020 at 21:00 UTC, from the C-404 simulations.** Cold cloud tops (brightness temperatures (Tb) $\leq$241 K) are used to mask out potential convective regions (black contours; A). Within these regions, areas with larger than 40 dBz composite reflectivity (Z) are used to identify areas with deep convection (red contours; B). Only wind speeds in the immediate surrounding of convective areas are considered to be straight line winds. Cold pool intensity (CPI) is shown in (D), potential maximum downdraft speeds (W_{down}) are shown in (E), potential maximum updraft speeds (W_{up}) are shown in (F), vertical wind speed at 91 m above groud (W91) are shown in (G), and vector shear between 10 m and 2.5 km above ground (VS2.5) are shown in (M).

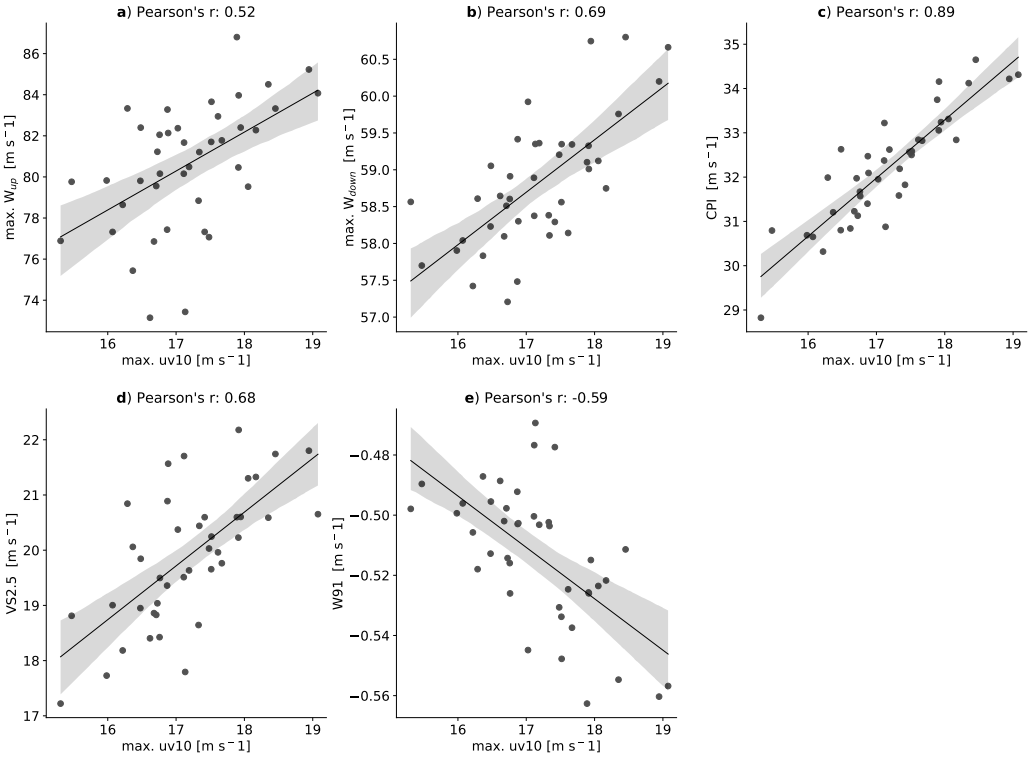

Fig. S 12: **The annual maximum of peak straight line wind (SLW) speeds is correlated with several predictor variables.** Correlation between JJA annual maximum of peak SLW speeds (max. uv10) and the annual maximum of the five predictor variables max. W_{up} (a), max. W_{down} (b), CPI (c), surface to 2.5 km above ground shear, and 91 m above ground downward windspeed. Black lines show the least square error linear regression between the variables and gray contours show the 95 % confidence intervals. The Pearson R correlation coefficient is shown in the title of each panel.

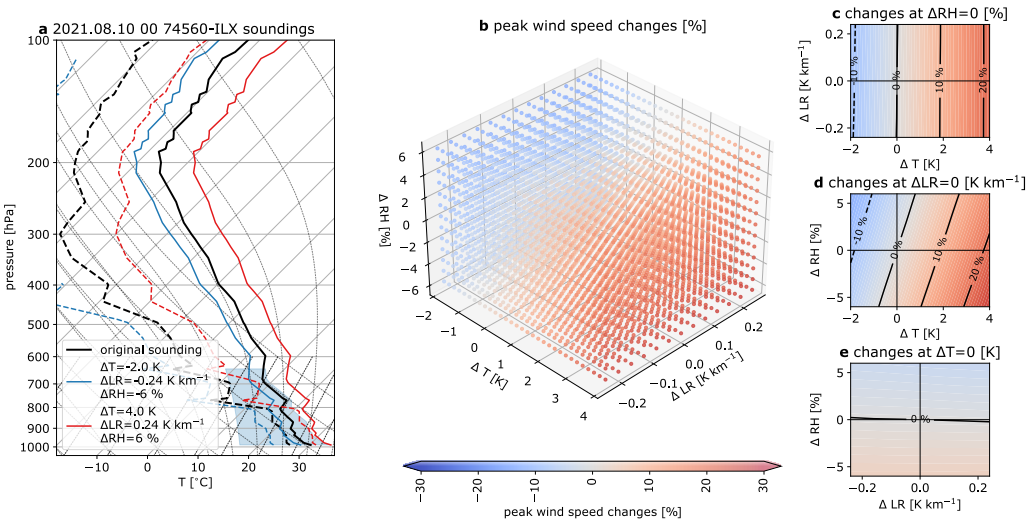

Fig. S 13: **Raising temperatures (T) systematically increase theoretical surface peak wind speeds in sounding staken before the passage of the Aug. 10 2021 midwest derecho while changes in relative humidity (RH) and temperature lapse rates (LR) have only minor impacts.** The 0 UTC sounding in Lincoln, IL on Aug. 10 2020 (a, black line) is systematically perturbed between -2 K and 4 K for T, -6 % to 6 % for RH, and -0.24 K km − 1 to 0.24 K km − 1 for LR and changes in DCAPE (blue region in a) are calculated. Solid lines in (a) show T and dashed lines show dewpoint temperatures. Blue lines show the maximum tested cooling and destabilization while red lines show the maximum warming and stabilization. Estimates for 10 m peak wind speed changes are shown in (b) for the entire change space. Panels c–e show changes when RH, LR, and T are kept constant, respectively.

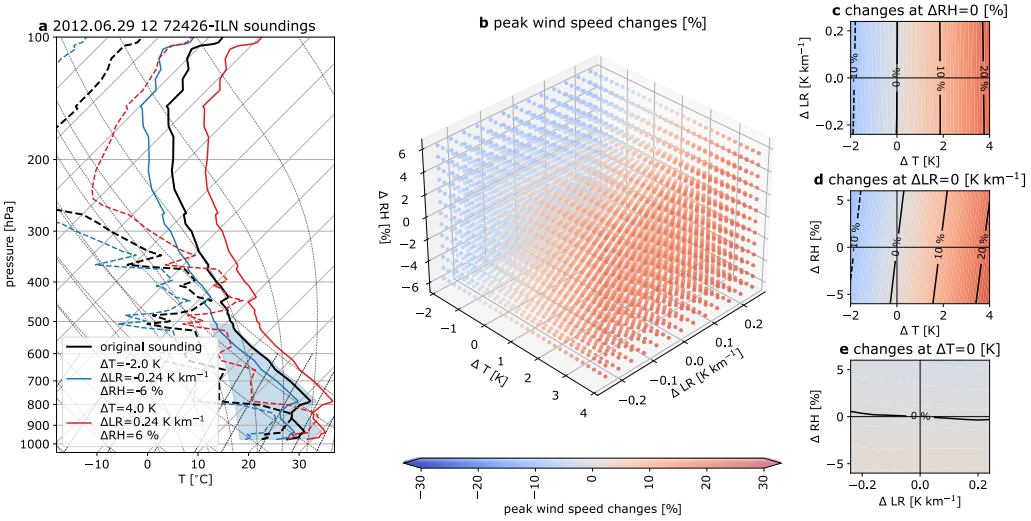

Fig. S 14: **Similar as Fig. S5 but for the Washington DC derecho on Jun. 29 2012 at 12 UTZ using the sounding from Wilmington, Ohio.**

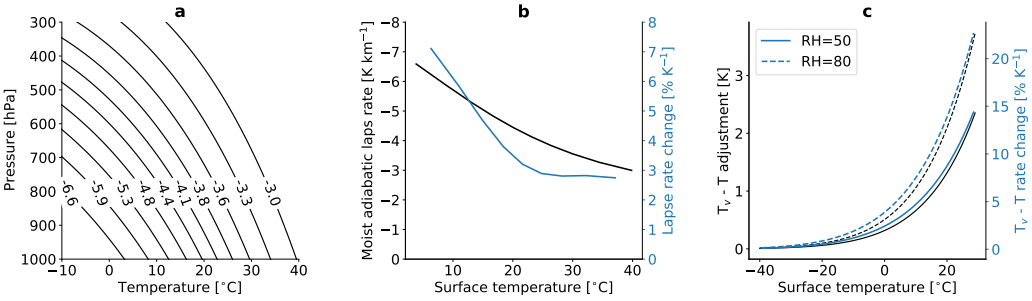

Fig. S 15: **Thermodynamic environmental conditions are becoming more favorable to support strong downdrafts in warmer atmospheres.** (a) Moist adiabatic descents as a function of temperature. The laps rates of the lowest 2 km in K km^{-1} is shown for each line. (b) Moist adiabatic lapse rate in the lowest 2 km as a function of surface temperature (black line) and correspondent changes with temperature (blue line; right y-axis). (c) Virtual temperature (T_v) corrections (T_v-T) as a function of surface temperature for relative humidities of 50 % (solid lines) and 80 % (dashed lines). Black lines show absolute corrections while blue lines show the change of the correction as a function of temperature (right y-axis).

1. Tun, T. N. & Than, A. Comparison of Wind Averaging Conversions between Gust Factor and Statistical Approaches. *International Journal of Scientific Engeneering and Technology Research* **7**, 2070–2076 (2014).